Letters in Applied NanoBioScience
Open-Access Journal (ISSN: 2284-6808)

*Article*
**Volume 15, Issue 3, 2026, 94**
https://doi.org/10.33263/LIANBS153.094

# DFT, ADME, Docking and Anti-inflammatory Activity of (*E*)-3-(3-Bromo-4-Methoxyphenyl)-1-(Substituted phenyl) Prop-2-en-1-ones

**Rajagopal Subha [1], Dr. Namasivayam Ingarsal [1,*]**

[1] Department of Chemistry, DG Govt. Arts College for Women (Affiliated to Annamalai University, Annamalainagar ), Mayiladuthurai, Tamil Nadu, India
[1] PG & Res. Department of Chemistry, Rajah Serfoji Govt. College (Autonomous) (Affiliated to Bharathidasan University, Trichy), Thanjavur, Tamil Nadu, India
* Correspondence: drningarsal@gmail.com (D.N.I.);

**Received: 17.01.2024; Accepted: 7.07.2024; Published: 02.07.2026**

**Abstract:** We have prepared two aryl α- and β-unsaturated ketones by microwave irradiation, and their formation is characterized by IR and NMR spectra. The DFT calculations are performed with the Gaussian 09 program using the B3LYP/6-311G(d,p) basis set. The structures of the present compounds are optimized. The existence of the trans-configuration in the present compounds is verified by proton NMR coupling constants and supported by a dihedral angle of 180° from DFT calculations. Their orbital energies and global descriptors are revealed. The NLO behavior of BMMP and BMDFP is calculated from their hyperpolarizabilities and found to be higher than that of standard urea's hyperpolarizability. Further, their ADME properties are studied using SwissADME and pkCSM tools, and the results are favorable for drug behavior. Docking with the COX-2 enzyme was performed using Autodock, and the binding affinity of the compounds to the enzyme was predicted (PDB ID: 3LN1). The *In vitro* study was also screened using the BSA method, and good inhibitory properties were observed.

**Keywords:** chalcones; IR and NMR spectra; DFT analysis; ADME behavior; docking; anti-inflammatory activity.



## 1. Introduction

In organic chemistry, a variety of functionalities with different linkages are reported in the literature, and their applications are widespread across different fields. Among those functionalities, compounds pertaining to α and β-unsaturated ketones are also included in such applications. Such compounds are called chalcones or prop-2-en-1-ones, and the name chalcone was given by Kostenecki [1]. In organic chemistry, these are used to synthesize pyrazoline [2], benzodiazepines [3], flavanones [4], isoxazoles [5], pyrimidines [6], etc. Several chalcones or aryl propenones act as good optical materials because of their higher hyperpolarizabilities than standard NLO materials like urea [7]. These are achieved by DFT calculations and other properties like the movement of electrons in frontier molecular orbitals with their energies, optimized structure, energies of electronic transitions from filled bonding to vacant non-bonding orbitals (NBO), electrostatic potentials, and charges associated with atoms (Mulliken) are also derived in the gas phase using the DFT approach with the Gaussian

09 package [8]. In the case of medicinal chemistry, they act as antimicrobials [9], anti-inflammatories [10], antiviral agents [11], proliferative activity [12], antioxidants, anticancer [13], etc. Nowadays, medicinal chemistry involves analyzing certain parameters computationally and their binding before *in vitro* or *in vivo* procedures. For the purpose of earlier investigation, the ADME behavior (absorption, digestion, metabolism, excretion) of a compound/drug is studied with the help of several web tools [14]. The activity and binding energies are computed by the molecular docking method [15]. These two studies are important before the *In vitro* assay of a drug to avoid failure and time consumption. By keeping these factors in mind, the author prepared two different substituted chalcones (BMMP and BMDFP) via microwave irradiation and characterized their formation using IR and NMR spectra. The DFT study of compounds (BMMP and BMDFP) is reported in this paper with the use of B3LYP/6-311G (d,p) basis set calculations. Before the *in vitro* anti-inflammatory assay, ADME properties were assessed using the SwissADME web tool, and the results were analyzed. Then, the molecular docking studies with COX-2 active site (PDB id: 3LN1) resulted in a good binding nature. Then, the *in vitro* anti-inflammatory activity is screened at three different concentrations.

## 2. Materials and Methods

*2.1. Preparation of (E)-3-(3-bromo-4-methoxyphenyl)-1-(4-methoxyphenyl)prop-2-en-1-one (BMMP).*

An equimolar quantity of 4'-methoxyacetophenone and 3-bromo-4-methoxy benzaldehyde is dissolved in 10ml of methanol and transferred to a 100ml pre-cleaned conical flask. Then, 3 ml of 40% KOH is added to it. This mixture is irradiated at 640W in a microwave oven [16], as shown in Scheme 1. Every 30 sec, the completion of the reaction is monitored by TLC. After 3 minutes, the reaction was completed as monitored by TLC and kept cool at room temperature. The formed precipitate is filtered and dried, then recrystallized from hot methanol. It yields glittering yellow needles of the desired product, and its melting point is noted. The same procedure is followed for preparing compound BMDFP for up to 3 minutes, and it also appeared as a pale yellow powder.

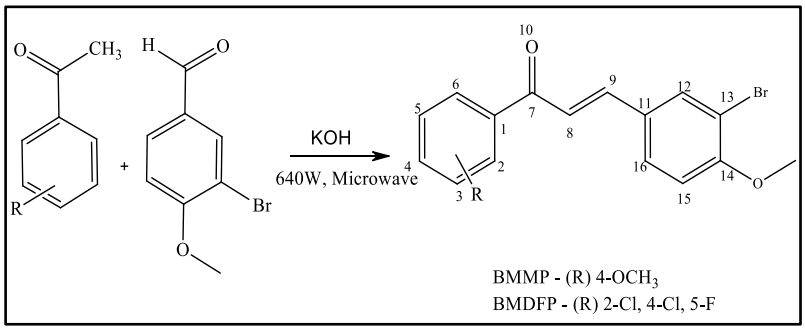


**Scheme 1.** Preparation of BMMP and BMDFP molecules.

*2.2. Instrumentation.*

The Spectrometer, AVATAR (model 330), was used for IR spectral measurements, and samples were measured as potassium bromide pellets.

For recording proton-resonance NMR spectra, a Bruker 400 NMR spectrometer operating at 400.23 MHz for $^{1}H$ and 100.62 MHz for $^{13}C$ was used for each NMR measurement.

*2.3. DFT analysis.*

Gaussian 09 program [8] is used to carry out the theoretical calculations with the B3LYP/6-311Gg (d,p) basis set. The structures are visualized in GaussView software. The present compounds are optimized using the B3LYP/6-311G(d,p) basis set.

*2.4. ADMET study.*

For the prediction of pharmacokinetic behavior for the present molecules, the SwissADME web tool and the pkCSM server are used.

*2.5. Molecular docking.*

The COX-II enzyme's 3D structure (PDB id:3LN1) was downloaded from the protein data bank, and the 3D structures of BMMP and BMDFP are optimized using the Gaussian 09W tool. Autodock vina [15] is used for docking studies, and their interactions are visualized using Biovia Discovery Studio 2017.

*2.6. In vitro assay.*

To assess the anti-inflammatory activity of the present molecules, BMMP and BMDFP, the bovine serum albumin denaturation technique [17] is used, along with the standard drug diclofenac sodium.

## 3. Results and Discussion

*3.1. Spectral characterization.*

The IR, proton, and carbon resonance spectra of the titled compounds are displayed in supplementary data as Figures S1, S2, S3, S4, S5, and S6.

3.1.1. (*E*)-3-(3-bromo-4-methoxyphenyl)-1-(4-methoxyphenyl)prop-2-en-1-one (BMMP).

Yield: 82%; pale yellow needles; mp:136-137°C, m/z 346; IR (KBr, νcm$^{-1}$) 1650 (CO), 1123 (CH$_{ip}$ ), 736 (CH$_{op}$), 1050 (CH=CH$_{op}$), 578 (C=C$_{op}$); $^{1}$H NMR (400 MHz, CDCl$_3$, δ/ppm) d 7.29(1H, *d*, J = 15.6 Hz), 7.701 (1H, *d*, J = 15 Hz), 3.897 (3H, s), 3.950 (3H, s), 6.918–8.051 (7H, overlapping *m*, ArH); $^{13}$C-NMR (100.64 MHz, CDCl$_3$, δ/ppm) 120.74 (C$_\alpha$), 132.52 (C$_\beta$), 188.38(CO), 56.41 (OCH$_3$), 55.52 (OCH$_3$), 111.86, 112.39, 163.45, 157.47, 142.16, 131.11, 130.79, 129.72, 113.55; Anal. Calcd. for C$_{17}$H$_{15}$BrO$_3$: C, 58.81; H, 4.35; Br, 23.01; O, 13.82.

3.1.2. (*E*)-3-(3-bromo-4-methoxyphenyl)-1-(2,4-dichloro-5-fluorophenyl)prop-2-en-1-one (BMDFP).

Yield 86%; mp 129-130°C; m/z 404; IR (KBr, νcm$^{-1}$) 1661 (CO), 1153 (CH$_{ip}$ ), 731 (CH$_{op}$), 1054 (CH=CH$_{op}$), 559(C=C$_{op}$); $^{1}$H NMR (400 MHz, CDCl$_3$, δ/ppm) d 6.972(1H, *d*, J = 15 Hz), 7.387 (1H, *d*, J = 15 Hz), 3.950 (3H, s), 6.915–7.798 (6H, overlapping *m*, ArH); $^{13}$C-NMR (100.64 MHz, CDCl$_3$, δ/ppm) 124.12 (C$_\alpha$), 145.26 (C$_\beta$), 190.80(CO), 111.94, 56.47 (OCH$_3$), 155.54, 158.23, 138.84, 133.30, 132.02, 129.81, 126.80, 117.39, 112.58. Anal. Calcd. for C$_{16}$H$_{10}$BrCl$_2$FO$_2$: C, 47.56; H, 2.49; Br, 19.78; Cl, 17.55; F, 4.70; O, 7.92.

*3.2. Computational study.*

3.2.1. Molecular structure, bond length, bond angle.

As shown in Figure 1, the structures of the molecules BMMP and BMDFP are displayed, both optimized to 100%. Due to the overall asymmetry, both BMMP and BMDFP are C1 point groups. The optimized energies for BMMP and BMDFP are -3453.8185 a.u. and -4339.0136 a.u, respectively. The calculated parameters from the geometrical optimization, such as bond angles and bond lengths of BMMP and BMDFP, are presented in Table S1 in the supplementary data. The carbonyl bond length (C7-O10) in BMMP and BMDFP is 1.26 Å. The olefinic bonds (C8-C9) in both BMMP and BMDFP are exactly the same at 1.35 Å. A good agreement was also observed between the bond lengths of the remaining atoms and those of the optimized structures. The bond angle data of both compounds are also in good agreement. The bond angles between C7-C8-C9 and O10-C7-C8 in BMMP and BMDFP are obtained as ~120°. It indicates that all compounds' enone moieties (α,β-unsaturated ketone) lie in the same plane. The dihedral angles of BMMP and BMDFP with O10-C7-C8-C9 and C7-C8-C9-C11 for all the present compounds are obtained as less than 2.230° and 180°, respectively. It clearly evidenced the presence of an E-configuration in the enone moiety. All bond lengths and angles are within the expected range and are consistent with previously reported chalcone structures [18].

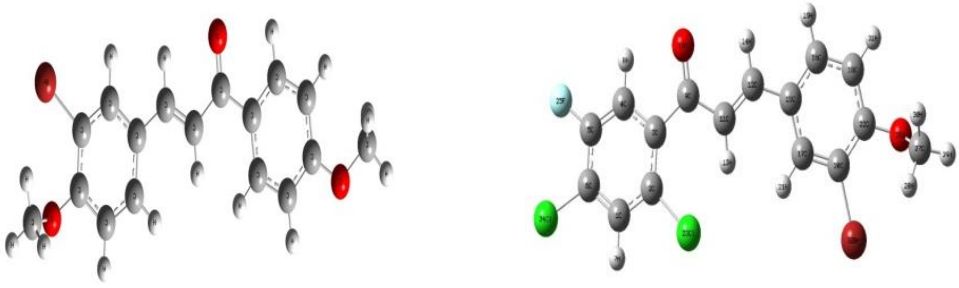

**BMMP** **BMDFP**

**Figure 1.** Optimized structures of synthesized BMMP and BMDFP.

3.2.2. HOMO-LUMO and reactivity descriptor's study.

Collectively referred to as FMO (frontier molecular orbitals), the combination of HOMO (highest occupied molecular orbital-donor) and LUMO (lowest unoccupied molecular orbital-acceptor) [19] provides valuable insight into the stability and reactivity of molecules. By analyzing the energy gap between FMOs, we can gain insight into the fundamental electronic properties of molecules. Figure 2 illustrates the HOMO-LUMO of BMMP and BMDFP compounds, with the former exhibiting a dispersed HOMO while the latter's HOMO is mainly concentrated on the enone and phenyl groups of the aldehyde.

The LUMO of both compounds is spread across almost the entire molecule, with the exception of the methyl groups linked to oxygen and halogens. **Table 1** presents the electronic parameters, revealing that BMMP has a significantly larger HOMO-LUMO energy gap than BMDFP, indicating a higher stability for BMMP. Additionally, the ionization potential and electron affinity values of BMDFP are greater than those of BMMP. Utilizing Koopman's theorem [20], global reactivity parameters such as chemical hardness (η), chemical softness (σ), global electrophilicity (ω), electronegativity (χ), and chemical potential (μ) have been calculated based on the HOMO-LUMO energy values. The chemical hardness and softness values suggest that both compounds are highly polarizable.

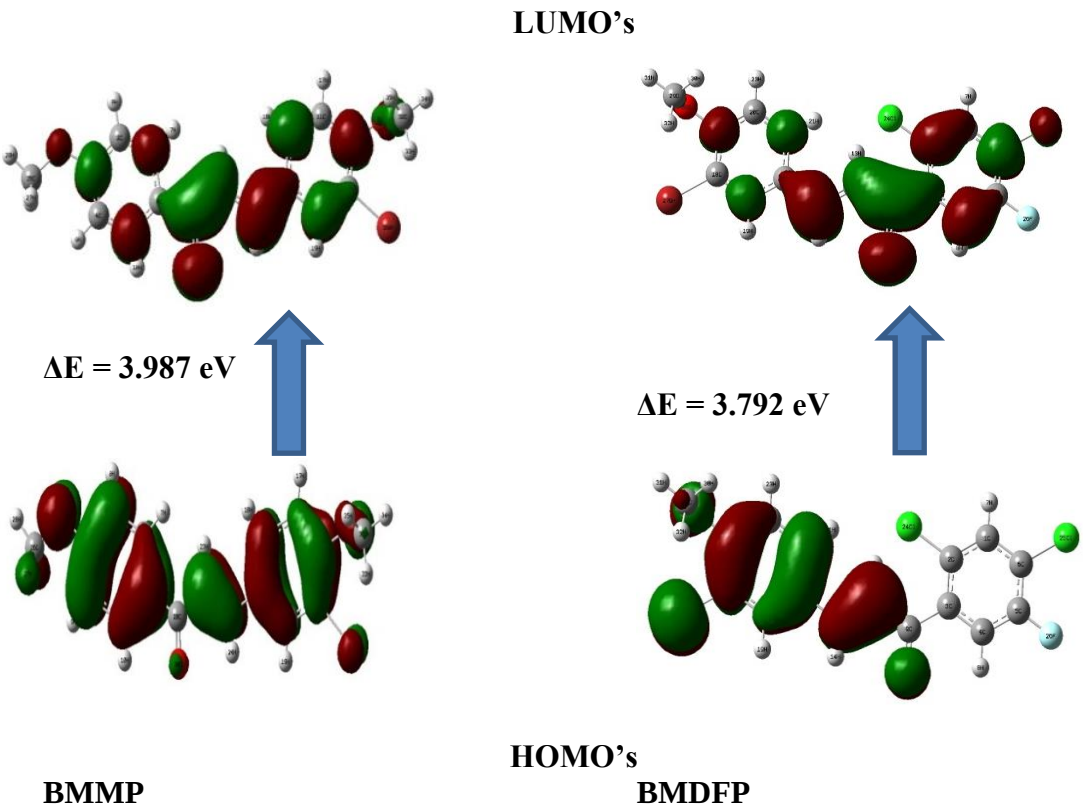


**Figure 2.** HOMO-LUMO's of BMMP and BMDFP.

**Table 1.** Electronic and global descriptors of BMMP and BMDFP.

| Electronic Parameters | BMMP | BMDFP |
|---|---|---|
| $E_{homo}$ (a u) | -6.208 | -6.571 |
| $E_{lumo}$ (a.u) | -2.221 | -2.779 |
| Energy gap (a.u) | 3.987 | 3.792 |
| Ionization energy (I) | 6.208 | 6.571 |
| Electron affinity (A) | 2.221 | 2.779 |
| Global reactivity parameters | BMMP | BMDFP |
| Global hardness (η) | 1.993 | 1.896 |
| Chemical potential (μ) | -4.215 | -4.675 |
| Electrophilicity index (ω) | 4.455 | 5.764 |
| Chemical softness (s) | 0.502 | 0.527 |

The chemical potential (μ) is associated with its electronegativity. The global electrophilicity index (ω) has a higher value for a good electrophile and a lower value for a good nucleophile. In the present investigation, BMDFP has a higher global electrophilicity index value and hardness, and is significantly more likely to accept electrons and undergo nucleophilic attack than BMMP. Additionally, the molecule BMDFP possesses excellent chemical strength and stability due to its higher electrophilicity, negative potential, and lower softness compared with BMMP.

NLO materials' involvement in electron delocalization is a significant concern for organic molecules. The charge transfer in intermolecular systems, which occurs as a result of electron cloud movement through the conjugated framework, is measured as the first hyperpolarizability ($\beta_0$), which is defined as the nonlinear optical activity of the molecular system. The equations (1) to (4) are used to compute the mean polarizability ($\alpha_0$), total static dipole moment (μ), and first-order hyperpolarizability ($\beta_0$). These values are based on observations of x, y, or z components.

$$\mu = (\mu_x^2 + \mu_y^2 + \mu_z^2)^{1/2} \text{ ..... (1)}$$

$$\alpha_0 = 1/3\ (\alpha_{xx} + \alpha_{yy} + \alpha_{zz}) \text{ ..... (2)}$$

$$\beta_0 = (\beta_x^2 + \beta y^2 + \beta z^2)1/2 \text{ ..... (3)}$$

$$\beta_0=[(\beta_{XXX}+ \beta_{XYY}+\beta_{XZZ})^2+(\beta_{YYY}+\beta_{YXX}+\beta_{YZZ})^2+(\beta_{ZZZ}+\beta_{ZXX}+\beta_{ZYY})^2]1/2\text{..... (4)}$$

For the current compounds, we calculated the total molecular dipole moment (μ) and first-order hyperpolarizability (β) using a 6-311G(d,p) basis set of the B3LYP method, and the values are given in Table 2.

**Table 2.** Dipole moments, polarizability, and hyperpolarizability of BMMP and BMDFP.

| **Dipole moment** | **BMMP** | **BMDFP** | **Hyperpolarizability** | **BMMP** | **BMDFP** |
|---|---|---|---|---|---|
| $\mu_x$ | 1.142 | 1.481 | $\beta_{xxx}$ | -57.26 | 221.157 |
| $\mu_y$ | 3.183 | -0.176 | $\beta_{xxy}$ | -8.679 | 7.808 |
| $\mu_z$ | 0.09 | 1.591 | $\beta_{xyy}$ | -70.621 | 62.32 |
| $\mu_{tot}$ (Debye) | 3.383 | 2.181 | $\beta_{yyy}$ | 14.091 | -79.117 |
| **Polarizability** | **BMMP** | **BMDFP** | $\beta_{xxz}$ | 62.599 | 68.562 |
| $\alpha_{xx}$ | -130.46 | -152.78 | $\beta_{xyz}$ | 42.668 | -1.739 |
| $\alpha_{xy}$ | 2.623 | 9.398 | $\beta_{yyz}$ | -2.845 | -2.03 |
| $\alpha_{yy}$ | -133.04 | -149.25 | $\beta_{xzz}$ | -56.037 | 28.23 |
| $\alpha_{xz}$ | 23.667 | 10.807 | $\beta_{yzz}$ | -6.665 | -25.377 |
| $\alpha_{yz}$ | -1.861 | -0.283 | $\beta_{zzz}$ | 6.661 | -0.934 |
| $\alpha_{zz}$ | -137.21 | -155.36 | $\beta_{\tau o \tau}$ (α.υ) | 195.546 | 332.885 |
| <α> (a.u) | 133.57 | 152.461 | $\beta_0$(esu) x $10^{-30}$ | 1.689 | 2.875 |
| $\alpha_{tot}$ (esu) x $10^{-24}$ | 19.795 | 22.595 | | | |

The significance of higher values of dipole moment (μ) and hyperpolarizability (β) for enhanced nonlinear optical properties is widely recognized. The first hyperpolarizability value of the BMDFP molecule (2.875x$10^{-30}$esu) is approximately nine times greater than that of urea (μ and β of urea are 1.3732 Debye and 0.3728×$10^{-30}$$cm^5$/esu) [22]. This indicates that the present compound, BMDFP, has better NLO characteristics than BMMP, whose hyperpolarizability (1.689x$10^{-30}$esu) is five times greater than that of urea. A high dipole moment in a molecule facilitates stronger dipole-dipole interactions among its atoms, leading to stronger intermolecular interactions. The BMMP molecule, with a higher dipole moment, exhibits considerably stronger intermolecular interactions than the BMDFP molecule.

3.2.3. MEP analysis.

The topography of the Molecular Electrostatic Potential (MEP) provides insights into the refined changes in the three-dimensional electronic distribution resulting from modifications in molecular structure. This is achieved by detecting and characterizing the MEP's critical points. The MEP of BMMP and BMDFP is calculated using the B3LYP/6-311G(d, p) method, and the results are depicted in Figure 3.

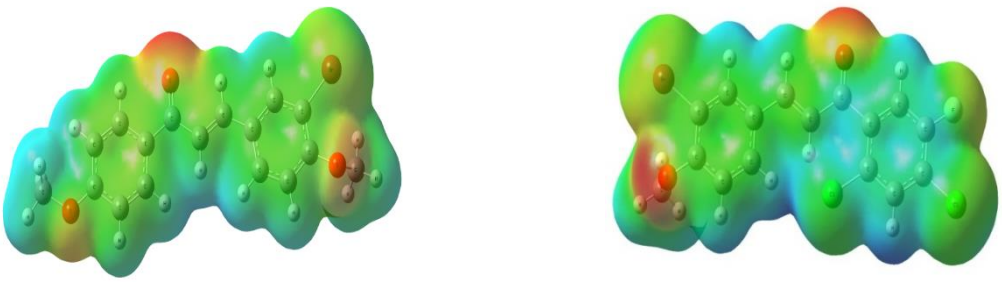

**BMMP** **BMDFP**

**Figure 3.** MEP illustration of BMMP and BMDFP.

The varying colors on the surface represent different electrostatic potential features; red indicates the highest electronegativity, blue represents the highest electropositivity, and green

indicates zero potential [23]. The potential follows the order of red, orange, yellow, green, and blue. In our study, the most electropositive region (blue, electron-poor) is located over the hydrogen atoms of the phenyl rings. The negative regions are localized in the bromo, carbonyl oxygen, and methoxy groups of both compounds, which act as electrophilic sites and can undergo electrophilic interactions.

3.2.4. NBO analysis.

The estimation of intra- and intermolecular bonding consequences is achieved using the natural bond orbital (NBO) analysis, which plays an essential role in investigating conjugative interactions and charge transfers within molecular structures. Interactions between donors and acceptors within a molecular organization stabilize the system by delocalizing electron density among occupied Lewis-type and unoccupied non-Lewis NBOs. Typically, π–π* orbital interactions exhibit higher energy values in comparison to σ–σ* interactions due to the large switch of electron density between the donor and acceptor moieties. To discover intra-molecular delocalization or hyperconjugation, the synthesized molecules are subjected to NBO evaluation at the DFT/B3LYP/6-311G(d,p) stage. The second-order Fock matrix was used to assess donor (i), acceptor (j), i.e., donor level bonds to acceptor stage bonds interplay inside the NBO evaluation as shown in equation (5), where each donor (i) and acceptor (j), the stabilization power E2 associates with the delocalization i → j E2.

$$E_2 = \Delta E_{i,j} = \left| \frac{qiF(i,j)^2}{\sum_i - \sum_j} \right| \quad \text{.....(5)}$$

Where qi is the donor orbital occupancy, Ei and Ej are diagonal elements, and F(i,j) is the off-diagonal NBO Fock matrix detail. The larger the $E_2$ cost, the more intensive, i.e., the greater the tendency of electron donors to donate to electron acceptors and the greater the quantity of conjugation of the entire device [24].

The C1–C2 bond electrons of both BMMP and BMDFP strongly undergo intra-molecular hyper-conjugation (π-π*) to the C3–C3 with the stabilization energies of 80.96 and 92.63 KJ/mol, respectively. The bonding electrons of C1–C2 undergo similar delocalization with anti-bonding vacant orbitals in carbonyl compounds (C7-O10), and the highest stabilization power is calculated for BMMP compared to BMDFP. Also, the sturdy hyperconjugation for BMMP takes place from π(C5-C6) of the donor to π*(C3-C4) of the acceptor. Within the case of BMDFP, a sturdy intra-molecular interplay between π(C8-C9) to π*(C7-O10) with the very best stabilization energies of 102.80 KJ/mol is found. The intramolecular interactions inside the molecules have caused the conjugated bonds in the molecules, which play a chief role in stabilizing the molecules. In the benzene ring, the ICT occurs with the aid of a switch of the π-electron cloud from donor to acceptor (π-π*), which ends up in the polarization of the molecules and the attribution of NLO properties. One of the fundamental participants in the resonance and interaction power inside the molecule is the electron donation from the LP(3)F5 of molecule BMDFP to BD*(2) C5 - C6 (n- π*), and these interactions result in a healthful stabilization energy of 105.31 KJ/mol. The stabilization energies inside the BMDFP are likewise raised via the presence of lone pair electrons in chlorine atoms. In addition, BMMP and BMDFP transfer a full-size amount of stabilization energies from non-bonding (Br13) to anti-bonding orbitals (C13-C14) throughout the n-π* transition. Each of the chalcones is further stabilized by the lone pair electron donation from

carbonyl oxygen (O10) to anti-bonding orbitals (n-σ*) of the vinyl part (C8-C9), with the extensive stabilization energies as shown in Table S2 in supplementary data. Based on the calculations of the maximal hyperconjugative power E(2), it's considerably noticeable that each molecule demonstrates higher suitability for packages within the fields of biology and medicine.

3.2.5. Mulliken population analysis.

The atomic charge distributions of the atoms present in compounds BMMP and BMDFP, as accomplished by Mulliken population analysis [25], are shown in Figure 4.

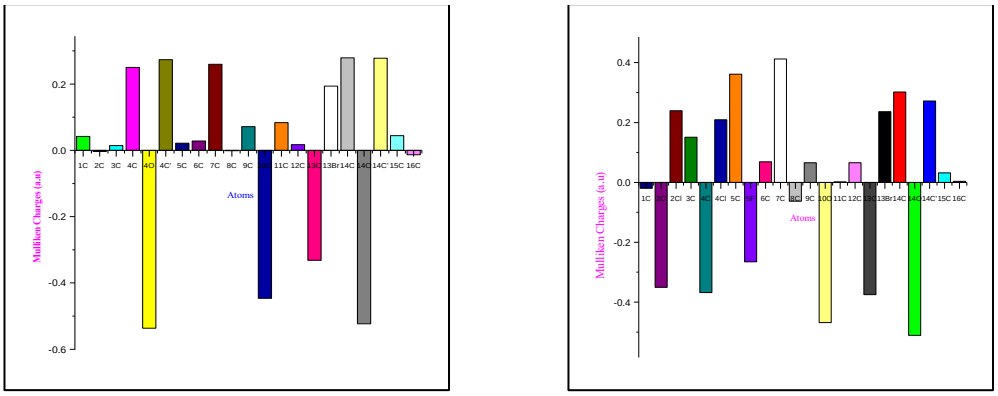


**Figure 4.** Bar graph of Mulliken charges for BMMP and BMDFP.

Mulliken atomic charges play a significant role in the application of quantum mechanical calculations to molecular structures. The theoretical calculation is used to depict the charge of every atom in the molecule. The distribution of positive and negative charges is necessary for the length of bonds between atoms to increase or decrease. In the present study, the oxygen atoms of BMMP and BMDFP are negatively charged because they are donor atoms. The oxygen atoms (O10) present in carbonyl groups display greater negative charges. Also, the oxygen atom ($O_4$) of the methoxy group in BMMP and the oxygen atoms O14 and O10 in the BMMP and BMDFP compounds have been shown to carry negative charges. The fluorine atoms in BMDFP have substantially shown negative charges. Carbon atoms exhibit a positive charge since they are acceptor atoms. The calculated Mulliken charges showed that there is more than one active center.

*3.3. Drug-likeness and ADME predictions.*

Considering that many drug development tasks fail throughout clinical trials due to bad ADME properties. So, it is vital to perform ADME checks at an early stage of drug discovery. Currently, SwissADME and pkCSM servers are used to analyze the ADMET residences of BMMP and BMDFP molecules. The drug-likeness of the existing BMMP and BMDFP molecules is predicted by following Lipinski's rule of 5 [26, 27]. It denoted that any drug molecule that is violet more than two of its criteria (molecular weight ≤ 500g/mol, number of hydrogen bond donors ≤ 5, a wide variety of hydrogen bond acceptors ≤ 10, calculated logP ≤ 5), the offer said drug molecule is taken into consideration as impermeable or weakly absorbed by the body.

By using and verifying this rule of five for the prevailing BMMP and BMDFP molecules from SwissADME and pkCSM internet tackle, as expected, as proven in Table S3

in supplementary data. The molecule BMMP has no violations and meets all criteria, whereas the molecule BMDFP has only one violation of the rule of 5, as defined by Lipinski. Subsequently, the titled molecules of each BMMP and BMDFP have demonstrated proper drug-likeness, oral bioavailability, and activity. The Bioavailability Radar for these compounds provides an overview of a molecule's drug-likeness (Figure 5). The region sketched in pink color suggests the range for each asset. FLEX for the power of the molecule as in step with rotatable bonds (≤9 bonds), size for the size because the molecular weight (among a 150–500 g/mol), POLAR for polarity as in line with the topological polar floor area (20–130 $Å^2$), INSOLU for insolubility in water via log S (≤6), and INSATU for saturation as in line with fraction of carbons within the sp3 hybridization (>0.25) [28].

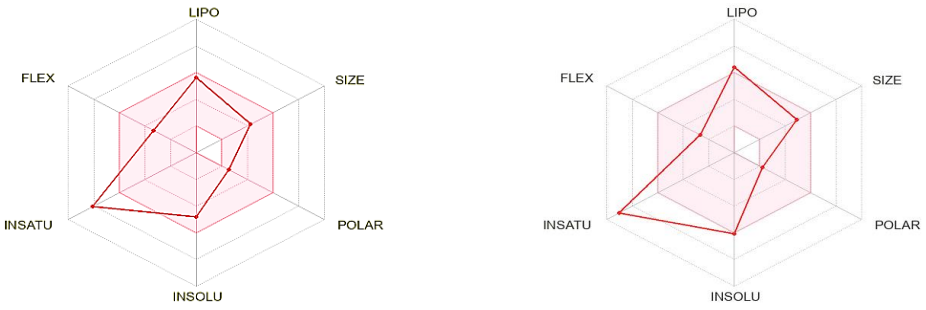


**BMMP** **BMDFP**

**Figure 5.** Bioavailability radar predictions for BMMP and BMDFP.

The radar depictions for the bioavailability of all the reported compounds are shown in Figure 5. The bioavailability radar prediction indicated that both molecules showed good lipophilicity, flexibility, size, and solubility. The fraction of Csp3 hybridization predictions is slightly beyond the radar level.

For absorption predictions, the parameters of skin permeability (log Kp), human intestinal absorption (HIA), and Pgp substrates are predicted. The skin permeability (log Kp) for BMMP and BMDFP are -2.381 and -2.477 cm/h, respectively, which are acceptable ranges. The HIA is 98.78 and 100 for BMMP and BMDFP, respectively, and it showed that they are predicted as well as absorbed molecules. P-glycoprotein can bind to a wide variety of substrates, which are widely distributed throughout the body. Pgp transporters are located inside the small gut, blood-brain barrier capillaries, and numerous crucial organs, including the kidney and liver [29]. The prevailing compounds BMMP and BMDFP aren't detected as Pgp substrates, and it is concluded that they do not affect the absorption, distribution, or clearance of substances and are properly metabolized.

Table S3 shows that both compounds exhibit volume of distribution (VDss) and blood-brain barrier (logBB) parameters within the acceptable limits. The VDss values for present BMMP and BMDFP molecules are predicted as 421 L/kg and 0.430 L/kg, respectively, and also showed moderate BBB behavior. These observations show that they are well distributed due to their strong plasma-binding properties and do not cause renal failure. Because these compounds are not inhibitors of the cytochrome enzymes CYP2D6 and CYP3A4, they may be metabolized, potentially increasing their elimination rate and decreasing their bioavailability in the body. These are isozymes of Cytochrome P450 enzymes, which are essential for the metabolism of many medications [30].

Total clearance is the result of eliminating the entire drug from the body. The amount of drug removed from the blood plasma in the vascular section per unit of time is called drug

clearance. In this study, the compounds of the present invention were well eliminated, as evidenced by very low overall clearance values (Table S3). All the compounds are predicted to be non-carcinogenic and non-mutagenic molecules. Also, they are e predicted to be non-hepatotoxic molecules. Overall, the titled compounds BMMP and BMDFP are predicted to be good drug-like molecules; hence, *in vitro* studies are carried out, especially on anti-inflammatory activities.

*3.4. Anti-inflammatory activity.*

The *in vitro* anti-inflammatory activities of recent molecules are carried out by using the BSA denaturation method [17] with diclofenac sodium as the standard drug. Inhibition screening is performed at five concentrations (20 µg/mL, 40 µg/mL, 80 µg/mL, 200 µg/mL, and 400 µg/mL), as shown in Table 3. The % inhibition of BMMP is excellent, as it is well above the standard inhibition values at all concentrations. The % inhibition of BMDFP is significantly lower than the standard and is considered to have good inhibitory properties for BMDFP and excellent inhibition properties for BMMP. It may be due to the presence of two methoxy electron donor groups, which facilitate the inhibitory property [31].

**Table 3.** Anti-inflammatory activity inhibition of BMMP and BMDFP.

| Molecules | Concentration (µg/mL) | % of inhibition |
|---|---|---|
| BMMP | 20 | 32.31 |
| | 40 | 39.45 |
| | 80 | 54.54 |
| | 200 | 62.28 |
| | 400 | 86.34 |
| BMDFP | 20 | 25.38 |
| | 40 | 33.33 |
| | 80 | 48.42 |
| | 200 | 57.59 |
| | 400 | 81.24 |
| Std (Diclofenac sodium) | 20 | 27.22 |
| | 40 | 35.37 |
| | 80 | 50.66 |
| | 200 | 59.33 |
| | 400 | 83.59 |

Both molecules have a tendency to prevent edema; however, BMMP has slightly greater potency than BMDFP. The graphical extract is shown in Figure 6.

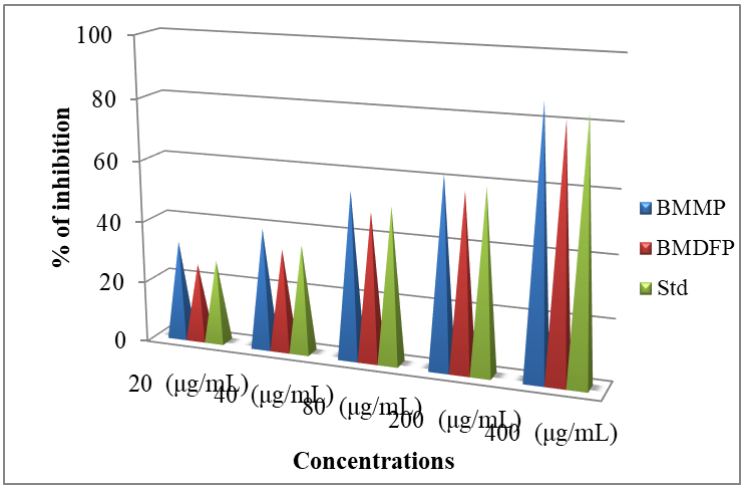


**Figure 6.** Graphical extract of *in vitro* anti-inflammatory activity.

*3.5. Molecular docking study.*

Molecular docking is performed for those compounds that showed better anti-inflammatory activity against the COX-2 protease protein 3LN1 to investigate their binding modes. The docking of present ligands with the 3LN1 receptor [32] is achieved with the help of Autodock Vina software [15].

Table 4 clearly indicates that both molecules exhibit good binding affinity and two hydrogen-bonding interactions in each case. The BMMP has slightly lower binding affinity than BMDFP (a more negative value indicates stronger binding). However, BMMP shows a strong interaction with the TYR371 amino acid residue, with its oxygen atom (1.7605 Å) attached to a methyl group. The molecule BMDFP has shown hydrogen-bonding interactions with ILE503, and both ligands have shown the same binding interactions with the PHE504 residue.

**Table 4.** Binding affinity and types of interactions from the docking result of BMMP and BMDFP.

| Ligands | Binding energy kcal/mol | Hydrogen Bonding interactions | | Hydrophobic interactions | |
|---|---|---|---|---|---|
| | | No. of interactions | Amino acid residue | No. of interactions | Amino acid residue |
| BMMP | -8.1 | 2 | TYR371 (1.7605A°) & PHE504 (3.1683A°) | 9 | Pi-sigma (LEU338, SER339 & VAL509), Alkyl (LEU370); Pi-Alkyl (PHE367, TYR371, TYR373 & VAL335); |
| BMDFP | -8.4 | 2 | ILE503 (2.9013A°) & PHE504(2.2175A °) | 14 | pi-sigma (GLN178, VAL335 & VAL509), Alkyl (ALA502, VAL509, ARG499, VAL102 & LEU345); Pi-Alkyl (HIS75-2, TYR341-2, ALA502, ALA513 & LEU517); |

Additionally, BMMP has shown 9 hydrophobic interactions, whereas BMDFP has shown 14 other interactions.

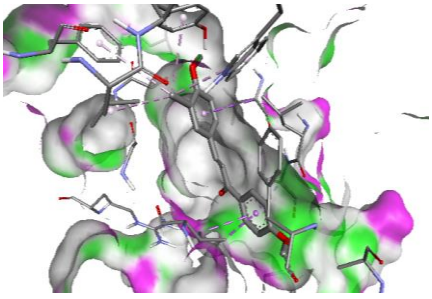

3D view (**BMMP**)

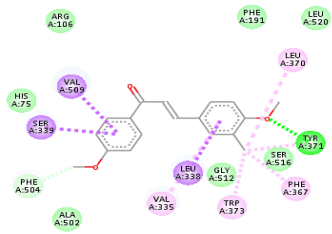


2D view (**BMMP**)

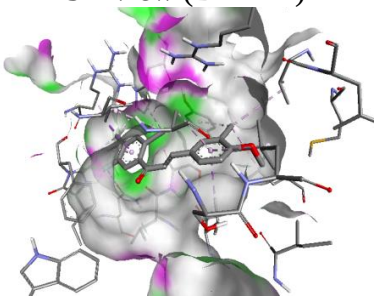

3D view (**BMDFP**)

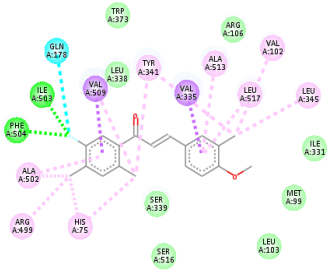


2D view (**BMDFP**)

**Figure 7.** 3D (surface around the ligand) and 2D (interactions) view of BMMP and BMDFP with 3LN1 receptor.

The interactions between ligands and receptors are shown in a 2D view, and their corresponding protein surfaces around the ligand poses are given a 3D view, as in Figure 7. Hence, both the present molecules tend to bind well with receptors and may display better biological performance.

## 4. Conclusion

Two diaryl α,β-unsaturated ketones have been synthesized from 3-bromo-4-methoxybenzaldehyde with 4-methoxyacetophenone and 2,4-dichloro-5-fluoroacetophenone by microwave irradiation, and the products are obtained within 3 min. Yields are 82% and 86% for BMMP and BMDFP, respectively. These physical constants are measured, and their IR and NMR spectral data characterize their formations. The carbonyl and its deformation modes are observed, and 1H NMR Spectral data confirm the existence of the trans form, which displays two doublets for the α- and β-protons with a coupling constant (J) of 16Hz in each case. The $^{13}$C NMR spectra were also recorded to confirm formation. The DFT investigation provides information on these compounds, including agreement of bond parameters with literature data and simulated spectral analysis that mostly coincides with experimental data. The dihedral angles of C7-C8-C9-C11 for both BMMP (180Å) and BMDFP (-179Å) have also supported the trans form α,β-unsaturated ketones. BMDFP is a better NLO material than BMMP due to its higher polarizability and stronger intramolecular interactions between π(C8-C9) and π*(C7-O10), with the highest stabilization energies of 102.80 kJ/mol and 75.86 kJ/mol observed for BMDFP and BMMP, respectively. In both cases, negative regions are localized in the bromo, carbonyl oxygen, and methoxy groups, which act as electrophilic sites and undergo electrophilic interaction. The Mulliken charges are calculated, and it is reported that oxygen atoms are observed with negative values. The physicochemical and ADME predictions showed that both molecules exhibit drug-likeness, supported by well-established anti-inflammatory activities i*n vitro* and in silico. The molecule BMMP has shown a better biological profile than the BMDFP molecule.

## Supplementary materials

The supplementary materials associated with this article are available here: **Download**

## Author Contribution

Conceptualization – R.S.; Software – R.S.; Formal analysis – R.S.; Investigation – N.I.; Validation – N.I.; Data curation – N.I.; Writing – original draft preparation – R.S.; Writing – review & editing – R.S., N.I. All authors have read and agreed to the published version of the manuscript.

## Informed Consent Statement

Not applicable.

## Institutional Review Board Statement

Not applicable.

## Data Availability Statement

Data supporting the findings of this study are available upon reasonable request from the corresponding author.

## Funding

This research received no external funding.

## Acknowledgments

The authors wish to thank the IR and NMR Facility, IACC, Gandhigram Rural Institute, Gandhigram, for recording the NMR and IR spectra of all compounds. Also, thank Bharathidasan University, Trichy.

## Conflicts of Interest

The authors declare no conflict of interest.

## References

1. Kostanecki, S.; Tambor, *J. Ber. Dtsch. Chem.* **1899**, *32*, 1921–1926, https://doi.org/10.1002/cber.18990320293.
2. Mehmood, R.; Sadiq, A.; Alsantali, R.I.; Mughal, E.U.; Alsharif, M.A.; Naeem, N.; Javid, A.; Al-Rooqi, M.M.; Chaudhry, G.E.; Ahmed, S.A. Synthesis and Evaluation of 1,3,5-Triaryl-2-Pyrazoline Derivatives as Potent Dual Inhibitors of Urease and α-Glucosidase Together with Their Cytotoxic, Molecular Modeling and Drug-Likeness Studies. *ACS Omega* **2022**, *7*, 3775−3795, https://doi.org/10.1021/acsomega.1c06694.
3. Rajkumar, T.; Suresh Kumar S.V.; Srinivasan, N. Ultrasonic Assisted Synthesis, Biological Evaluation, and Molecular Docking of Chalcone-based 1,5-benzodiazepine as Potential Anticonvulsant Agents. *Curr. Enz. Inhib*. **2022**, *18* 32-39, https://doi.org/10.2174/1573408018666220224145245.
4. Leonte, D.; Ungureanu, D.; Zaharia, V. Flavones and Related Compounds: Synthesis and Biological Activity. *Molecules* **2023**, *28*, 6528, https://doi.org/10.3390/molecules28186528.
5. Fandakli, S. Turk. Synthesis of some new isoxazole compounds and their biological tyrosinase and antioxidant activities. *J. Chem.* **2022**, *46*, 747-753, https://doi.org/10.55730/1300-0527.3364.
6. Ali hazam, M.; Mahesein, R.J.; AL-Salman, H.N.K. Synthesis and characterization of Pyrimidine from chalcone as a polymeric prodrug with fusidic acid and ZnO and study bioactivityJ. *Popul. Ther. Clin. Pharmacol.* **2023**, *130*, e156–e175, https://doi.org/10.47750/jptcp.2023.30.05.018.
7. Mohammed, M.; Khairul, W.M.; Rahamathullah, R.; Razak, F.I.A.; Sapari, S. Synthesis, photophysical and computational approaches on nonlinear optical (nlo) properties of naphthalen-1-yl ethynylated-chalcone derivative. *Malay. J. Ana. Sci*. **2022**, *26*, 684 – 697.
8. Frisch, M. M.J.; Trucks, G.W.; Schlegel, H.B.; Scuseria, G.E.; Robb, M.A.; Cheeseman, J.R.; Scalmani, G.; Barone, V.; Mennucci, B.; Petersson, G.A.; Nakatsuji, H.; Caricato, M.; Li, X.; Hratchian, H.P.; Izmaylov, A.F.; Bloino, J.; Zheng, G.; Sonnenberg, J.L.; Hada, M.; Ehara, M.; Toyota, K.; Fukuda, R.; Hasegawa, J.; Ishida, M.; Nakajima, T.; Honda, Y.; Kitao, O.; Nakai, H.; Vreven, T.; Montgomery Jr. J.A.; Peralta, J.E.; Ogliaro, F.; Bearpark, M.; Heyd, J.J.; Brothers, E.; Kudin, K.N.; Staroverov, Keith, T.; Kobayashi, R.; Normand, J.; Raghavachari, K.; Rendell, A.; Burant, J.C.; Iyengar, S.S.; Tomasi, J.; Cossi, M.; Rega, N.; Millam, J.M.; Klene, M.; Knox, J.E.; Cross, J.B.; Bakken, V.; Adamo, C.; Jaramillo, J.; Gomperts, R.; Stratmann, R.E.; Yazyev, O.; Austin, A.J.; Cammi, R.; Pomelli, C.; Ochterski, J.W.; Martin, R.L.; Morokuma, K.; Zakrzewski, V.G.; Voth, G.A.; Salvador, P.; Dannenberg, J.J.; Dapprich, S.; Daniels, A.D.; Farkas, O.; Foresman, J.B.; Ortiz, J.V.; Cioslowski, J.; Fox, D.J. Gaussian 09, Revision D.01, Gaussian, Inc, Wallingford CT, **2013**.
9. Maurya, A.; Agrawal, A. Recent Advancement in Bioactive Chalcone Hybrids as Potential Antimicrobial Agents in Medicinal Chemistry. *Mini. Rev. Med. Chem.* **2024**, *24*, 176-195, https://doi.org/10.2174/1389557523666230727102606.

10. Kumar, V.; Lal, K.; Tittal Naveen, R.K. The fate of heterogeneous catalysis & click chemistry for 1,2,3-triazoles: Nobel prize in chemistry 2022. *Catal. Commun*. **2013**, *176*, 106629, https://doi.org/10.1016/j.catcom.2023.106629.
11. Zhan, W.; Mao, P.; Yuan, C.; Zhang, Y.; Zhang, T.; Liu, Y.; Tian, J.; Xue, W. Design, synthesis and antiviral activities of chalcone derivatives containing pyrimidine. *J. Saud. Chem. Soc*. **2023**, *27*, 101590, https://doi.org/10.1016/j.jscs.2022.101590.
12. Li, J.; Fan, P.; Liu, Y.; Zhao, Y.; Shi, C.; Zhou, S.; Qiu, H. Design, synthesis, and antiproliferative activity of novel 1,2,4-triazole-chalcone compounds**.** *Heterocyclic Communications*. **2023**, *29*, 20220165, https://doi.org/10.1515/hc-2022-0165.
13. Siddiqa, A.; Tajammal, A.; Irfan, A.; Azam, M.; Ali Munawar, M.; Hardy, R.S.; Raza Basra, M.A. Synthesis, molecular docking, bio-evaluation and quantitative structure activity relationship of new chalcone derivatives as antioxidants. *J. Mol. Str*. **2023**, *1127*, 134814, https://doi.org/10.1016/j.molstruc.2022.134814.
14. Ardal, C.; Alstadsæter, A.; Røttingen, J.A. Common characteristics of open source software development and applicability for drug discovery: a systematic review. *Health Res. Policy Syst*. **2011**, *9*, 36, https://doi.org/10.1186/1478-4505-9-36.
15. Trott, O.; Olson, A.J. AutoDock Vina: Improving the speed and accuracy of docking with a new scoring function, efficient optimization, and multithreading. *J. Comput. Chem.* **2010**, *31*, 455-461, https://doi.org/10.1002/jcc.21334
16. Yadav, D.K.; Kaushik, P.; Pankaj, Rana, V.S.; Kamil, D.; Khatri, D.; Shakil, N.A. Microwave Assisted Synthesis, Characterization and Biological Activities of Ferrocenyl Chalcones and Their QSAR Analysis. *Front. Chem*. **2019**, *7*, 814, https://doi.org/10.3389/fchem.2019.00814.
17. Lavanya, A.; Sribalan, R.; Padmini, V. Synthesis and biological evaluation of new benzofuran carboxamide derivatives. *J. Saudi Chem. Soc.* **2017**, *21*, 277-285, https://doi.org/10.1016/j.jscs.2015.06.008.
18. Adole, V.A. DFT calculations on three 2,3-dihydrobenzofuran linked chalcones: Structural, HOMO-LUMO and spectroscopic (UV-Vis and IR) interpretation. *Vietnam J. Chem.* **2023**, *61*, 147-157, https://doi.org/10.1002/vjch.202100023.
19. Mishra, R.; Srivastava, A.; Sharma, A.; Tondon, P.; Baraldi, C.; Gameroni, M.C. *Spectrochim. Acta. Mol. Biomol. Spectrosc.* **2013**, *101*, 335–342. https://doi.org/10.1016/j.saa.2012.09.092.
20. Koopmans, T.A. Über die Zuordnung von Wellenfunktionen und Eigenwerten zu den Einzelnen Elektronen Eines Atoms. *Physica* **1934**, *1*, 104–133, https://doi.org/10.1016/S0031-8914(34)90011-2.
21. Custodio, J.M.F.; D'Oliveira, G.D.C.; Gotardo, F.; Cocca, L.H.Z.; de. Boni, L.; Perez, C.N.; Napolitano, H.B.; Osorio, F.A.P.; Valverde, C. Second-order nonlinear optical properties of two chalcone derivatives: insights from sum-over-states. *Phy. Chem. Chemic. Phys.* **2021**, *23*, 6128-6140, https://doi.org/10.1039/D0CP06469F.
22. Shruthi, C.; Ravindrachary, V.; Guruswamy, B.; Prasad, D.J.; Goveas, J.; Kumara, K.; Lokanath, N.K. *J.* Molecular structure, Hirshfeld surface and density functional theoretical analysis of a NLO active chalcone derivative single crystal—A quantum chemical approach. *Mol. Str.* **2021**, *1228*, 129739, https://doi.org/10.1016/j.molstruc.2020.129739.
23. Baig, H.; Iqbal, A.; Rasool, A.; Hussain, S.Z.; Iqbal, J.; Alazmi, M.; Alshammari, N.; Alazmi, A.; AlGhadhban, A.; Sulieman, A.M.E.; Said, K.B.; Rehman, H.; Saleem R.S.Z. Synthesis and Photophysical, Electrochemical, and DFT Studies of Piperidyl and Pyrrolidinyl Chalcones. *ACS Omega* **2023**, *8*, 28499-28510, https://doi.org/10.1021/acsomega.3c02813.
24. Hugas, D.; Simon, S.; Duran, M. Electron Density Topological Properties Are Useful To Assess the Difference between Hydrogen and Dihydrogen Complexes. *The J. Phy. Chem*. **2007**, *111*, 4506–4512, https://doi.org/10.1021/jp070080u.
25. Gunasekaran, S.; Kumaresan, S.; Arunbalaji, R.; Anand, G.; Srinivasan, S. Density functional theory study of vibrational spectra, and assignment of fundamental modes of dacarbazine. *J. Chem. Sci.* **2008**, *120*, 315–324, https://doi.org/10.1007/s12039-008-0054-8.
26. Lipinski, C.A. Rule of five in 2015 and beyond: Target and ligand structural limitations, ligand chemistry structure and drug discovery project decisions. *Adv. Drug. Deliv. Rev*. **2016**, *101*, 34–41. https://doi.org/10.1016/j.addr.2016.04.029.
27. Saini, N.; Grewal, A. S.; Lather, V.; Gahlawat, S. K. Natural alkaloids targeting EGFR in non-small cell lung cancer: Molecular docking and ADMET predictions. *Chemico-Biological Interactions*. **2022**, *358*, 109901, https://doi.org/10.1016/j.cbi.2022.109901.

28. Daina, A.; Michielin, O.; Zoete, V. SwissADME: a free web tool to evaluate pharmacokinetics, drug-likeness and medicinal chemistry friendliness of small molecules. *Sci. Rep.* **2017**, *7*, 42717, https://doi.org/10.1038/srep42717.
29. Tan, D.S. Current Progress in Natural Product-like Libraries for Discovery Screening. *Comb. Chem. High. Throughput Screen*. **2004**, *7*, 631–643, https://doi.org/10.2174/1386207043328418.
30. Sychev, D.A.; Md Ashraf, G.; Svistunov, A. A.; Maksimov, M.L.; Tarasov, V.V.; Chubarev, V.N.; Otdelenov, V.A.; Denisenko, N.P.; Barreto, G.E.; Aliev, G. The cytochrome P450 isoenzyme and some new opportunities for the prediction of negative drug interaction in vivo. *Drug. Des. Devel. Ther*. **2018**, *12*, 1147-1156, https://doi.org/10.2147/DDDT.S149069.
31. Rohini, R. M.; Devi, K.; Devi, S. Synthesis of novel phenyl azo chalcone derivatives for antitubercular, antiinflammatory and antioxidant activity. *Der Pharma Chemica*. **2015**, *7*, 77-83.
32. Mittal, R.; Sharma, S.; Mittal, A.; Kumar, S.; Kushwah, A. S. Virtual Screening, Molecular Docking, and Physiochemical Analysis of Novel 1,3-diphenyl-2-propene-1-one as Dual COX-2/5-LOX Inhibitors. *Lett. Drug Des. Discov*. **2022**, *21*, 270-288, https://doi.org/10.2174/1570180819666220523093435.

## Publisher's Note & Disclaimer